Seasonal and diurnal variability in air pollutants and short-lived climate forcers measured at the Rwanda Climate Observatory

H. Langley DeWitt[1], Jimmy Gasore[1,3,4], Maheswar Rupakheti[2], Katherine E. Potter[1], Ronald G. Prinn[1], Jean de Dieu Ndikubwimana[3], Julius Nkusi[3], and Bonfils Safari[4]

[1] Massachusetts Institute of Technology, Center for Global Change Science, Cambridge, MA, USA

[2]Institute for Advanced Sustainability Studies (IASS), Potsdam, Germany

[3]Ministry of Education, Climate Secretariat, Kigali, Rwanda

[4]Unviersity of Rwanda, Physics Department, Kigali, Rwanda

Abstract

Air pollution is still largely unstudied in sub-Saharan Africa, resulting in a gap in scientific understanding of emissions, atmospheric processes, and impacts of air pollutants in this region. The Rwanda Climate Observatory, a joint partnership between MIT and the government of Rwanda, has been measuring ambient concentrations of key long-lived greenhouse gases and short-lived climate-forcing pollutants (CO_2, CO, CH_4, BC, O_3) with state-of-the-art instruments on the summit of Mt. Mugogo (1.586° S, 29.566° E, 2590 m above sea level) since May 2015. Rwanda is a small, mountainous, and densely populated country in equatorial East Africa, currently undergoing rapid development but still at less than 20% urbanization. Black carbon concentrations during Rwanda's two dry seasons, which coincide with the two biomass burning seasons, are higher at Mt. Mugogo than in major European cities with daily averages of 5 $\mu g\ m^{-3}$. BC baseline concentrations during biomass burning seasons are loosely correlated with fire radiative power data for the region acquired with MODIS satellite instrument. The position and meteorology of Rwanda is such that the emissions transported from both the northern and southern African biomass burning seasons affect BC, CO, and O_3 concentrations in Rwanda. Spectral aerosol absorption measured with a dual-spot Aethalometer varies seasonally due to changes in types of fuel burned and direction of pollution transport to the site. Ozone concentrations peaked during Rwanda's dry seasons (daily measured maximum of 70 ppbv). Understanding and quantification of the percent contributions of regional and local (beyond large-scale biomass) emissions is essential to guide policy in the region. During the rainy season, local emitting activities (e.g., cooking, transportation, trash burning) remain steady, regional biomass burning is low, and transport distances are shorter as rainout of pollution occurs regularly. Thus local pollution at Mugogo can be estimated during this time period, and was found to account for up to 35% of annual average BC measured. Our measurements indicate that air pollution is a current and growing problem in equatorial East Africa that deserves immediate attention.

1. Introduction

According to recent data collected and published by the World Bank, particulate air pollution in most African countries is above the annual average guideline values recommended by the World Health Organization (WHO). Despite this, little scientific research has been published on air quality in Africa (Figure 1). The WHO reports that one in eight premature deaths globally can be linked currently to poor air quality, and these deaths are concentrated in developing countries (WHO, 2013). Black carbon (BC) is one of the major air pollutants emitted from Africa,

mainly from biomass burning as it is widespread on the continent during certain seasons. In addition to affecting health, BC contributes to atmospheric heating and thus to climate change(Ramanathan and Carmichael, 2008). Widespread crop fires in northern and southern Africa, prevalent in boreal winter (December-January-February, DJF) and astral winter (June-July-August, JJA), respectively, are known to increase aerosol and ozone concentrations in this region and transported molecular and aerosol fire tracers associated with elevated ozone have been measured as far as the Pacific and Indian Oceans (Field et al., 2016; Real et al., 2010).

Rwanda is located in the middle of the two major seasonal biomass burning regions of sub-Saharan Africa. Wide-scale biomass burning occurs to the north of Rwanda during December-January-February (DJF) and to the south during June-July-August (JJA). Rwanda's climate may exacerbate fire haze pollution effects, as Rwanda experiences two dry seasons that occur at the same time as these two continental burning seasons, making long range transport with low rainout efficiency likely. Rwanda's prevalent wind direction also changes from northerly (DJF) to southerly (JJA) at the same time as the large-scale biomass burning area shifts from north-central Africa to southern Africa. Increase in incidence and amount of biomass burning is thought to be one consequence of climate change in this region (Niang et al., 2014). Southern Africa's biomass burning is also influenced significantly by human activity, not just the climate (Archibald et al., 2010). Rwanda is positioned to experience both large-scale (transported) haze due to fires and human activities and local, diffuse emissions.

In addition to air quality issues, climate change (related to air pollution) may also adversely affect Rwanda, and the major pollutants from or ultimately increased by biomass burning (particles, carbon monoxide, ozone) are also known climate forcers. The main products exported (coffee and tea), the livelihood of the majority of Rwandans (agriculture), and power (currently almost half of Rwanda's power is hydroelectric) are all potentially affected by climate change. These issues are similar across the region. Central Africa is expected to receive increased severe rainstorms, which may lead to erosion and an uptick in vector-borne diseases (Niang et al., 2014). Rwanda's mountainous topography and ubiquitous hillside agriculture makes Rwanda venerable to floods and landslides. However, there is limited on-ground data on air quality and climate change in Africa.

In order to advance our scientific understanding of air pollution, climate change, and their impacts in Africa through generation of on-the-ground data, MIT and the government of Rwanda have established the Rwanda Climate Observatory (RCO) to measure long-lived greenhouse gases and short-lived climate forcers/pollutants in East Africa. Since May 2015, CH_4, CO, CO_2, O_3, and BC concentrations have been continuously measured, and N_2O measurements were added in February 2017. The RCO is a part of the Advanced Global Atmospheric Gases Experiment (AGAGE) network, a global network of high-frequency trace greenhouse gas measurements (Prinn et al., 2000), and is the first station of its kind in Africa. Rwanda was chosen as a location due to several factors:, including government interest from Rwanda and willingness to take on station maintenance, Rwanda's interest in growing its technical sector, specifically focused on green growth,

Rwanda's high and mountainous terrain, which means that stations located in Rwanda could measure pollution transported from the East and Central Africa region, readily available infrastructure in Rwanda to support the project, and a gap in climate data in this area of the world .

Here we present first results on diurnal and seasonal variations in short-lived climate forcers/pollutants related to air quality, focusing on O_3, CO, and BC observed at the RCO, and discuss variations and air pollution sources. This dataset is unique and unprecedented to the region and this information on overall concentrations, sources, and time-dependent concentration variations of these air pollutants is essential in this rapidly changing area of the world to not only advance our understanding of air pollution and climate change in the region but also inform future policies on air pollution with sound science.

2. Experimental Methods: Rwanda Climate Observatory

2.1 Rwanda Climate Observatory Environment

The RCO is located in the Northern Province of Rwanda, near Byangabo on the summit of Mt. Mugogo (1.586° S, 29.566° E, 2590 m above sea level). Mt. Mugogo is about 70 km (aerial distance) to the north-west from Kigali, the capitol of Rwanda (population of approximately 1 million), 20 km (south-west) from the next major city, Musanze (population of around 100,000), and 60 km north-east from the Lake Kivu region (Gisenyi, Rwanda and Goma, DRC, combined population of approximately 1 million). A dirt road reaches the base of the mountain, about 500 m below the summit where the RCO is located, and a diesel generator is installed on the road at the base.

Inlets were installed on both the roof of the Observatory (10 m above ground level) for O_3 and BC) and on a Rwanda Broadcasting Authority Tower (35 m above ground level) for CO, CO_2 and CH_4. There is a small Rwandan army camp adjacent to the measurement site and a eucalyptus forest and a mix of agricultural fields and scattered rural houses surround the immediate vicinity of the RCO (Figure 2).

The high altitude and remote positioning of Mt. Mugogo allows sampling of regional air masses from throughout East Africa depending on prevailing meteorological conditions, as well as local pollution (as the dense population but low urbanization of Rwanda means that direct human influence is ubiquitous except within the national parks). Kigali and the Lake Kivu region are approximately 1000 m in altitude below the station height and their altitude (~1500 m) can be used as the base of local pollution. The majority of air masses transported to Mugogo originate below 5 km above ground level. Approximately 20% of yearly air masses measured at Mugogo's summit originate from 0-1 km above ground level, and approximately 36% below 2 km (from HYSPLIT analysis). During mid-day, Mugogo's summit is likely within the regional polluted boundary layer, but at other times of the day it is above. Complicating this issue is the network of farms and houses along the mountainside near Mt. Mugogo.

2.2 Instrumentation

Details on the instruments sampling at the RCO are compiled in Table 1. PM2.5 BC (particulate matter 2.5 micrometers in diameter or less) was measured using a Magee Scientific 7-wavelength Aethalometer with dual-spot technology that is able to

correct for filter loading artifacts (Drinovec et al., 2015). A cyclone PM2.5 impactor was installed on the inlet to remove larger particles. Air was passed through a filter once per day to collect blank data. Flow was calibrated once per year and after major instrument movement and changes, while the optical performance was calibrated with a neutral density filter kit once per year. Data was recorded every minute at a 5 liter per minute (LPM) flow rate and particles were captured on a quartz fiber filter tape. The air stream was not dried and the relatively humidity (RH) was not controlled, which could lead to increased uncertainty during periods of high relative humidity. RH recorded at the station varied by approximately 5% over the day and from 60-85% monthly, depending on the season. The 880 nm channel was used to calculate the concentration of BC.

CO mixing ratios were measured in real-time using a cavity ring-down spectrometer (G2401, Picarro, USA). Sampled, laboratory, and calibration air were dried with a Nafion drier inside an Earth Networks calibration box to increase the accuracy of the Picarro water vapor correction (Welp et al., 2013). Three NOAA-standard calibration tanks were used for calibration spanning normal ambient concentrations and calibrations were performed once per day initially to check for linearity of instrument's response (Gasore, 2018). An O_3 monitor (T400, Teledyne Advanced Pollution Instrument, USA) was used to measure O_3. Regular checks were performed using internal span and zero O_3 calibrations. Flow was calibrated two to three times per year.

Meteorological data (ambient temperature, relative humidity, pressure, wind speed, wind direction and rainfall) were collected with an automatic weather station

(WXT520, Vaisala, Finland). The weather station was attached to a fixed, hinged arm 35 m above ground level and connected to the communications tower, level with the $CO/CO_2/CH_4$ inlet, with a 2 m clearance from the tower.

3. Results and Discussion

3.1 Seasonal Variation in BC, CO, and O_3

Figure 3 shows a summary of the data, including daily and 15 minute averaged BC , O_3, and CO data and meteorological data. Daily averages were examined to probe overall increases in regional pollutants, while 15 minute averages were used to detect local pollution. Five minute data (not pictured) was used to detect very local pollution and remove influence of short-lived local fires and BC from the generator 500 m below the station. Spikes in BC concentrations that lasted for less than 15 minute with values higher than 25,000 ng m^{-3} were removed, along with corresponding CO.

Rwanda has two rainy seasons roughly occurring in March-April-May (MAM) and September-October-November (SON), and two dry seasons during December-January-February (DJF) and June-July-August (JJA). This generalized definition and durations of the seasons are used the purpose of comparing data for multiple years and is used throughout this paper. High variations in BC concentrations can be seen in the BC time series (Figure 3) ranging from below 100 to above 20,000 ng m^{-3}, with an average value of 1,700 ng m^{-3} (standard deviation: 1,600 ng m^{-3}). Peak concentrations corresponded to dry seasons. CO and O_3 mixing ratios also increased during the dry seasons compared to the rainy seasons, though not as pronounced as the BC increases. This is partially due to the efficient rainout of black carbon particles during

187 the rainy season. The diurnal, weekly, and monthly variations in concentrations of
188 each species, normalized to their average, are shown in Figure 4.
189 It has been known for some time that wide-scale biomass burning in sub-
190 Saharan Africa has a large seasonal effect on the atmosphere (Archibald et al., 2010;
191 Crutzen and Andreae, 1990). Understanding and separating these seasonal effects
192 from anthropogenic emissions can be difficult without continuous data sets both
193 during and outside of this period, especially as both biomass burning and
194 anthropogenic emissions in this region of the world emit BC, CO, and PM, and
195 anthropogenic emissions contain O_3 precursors that can increase O_3 formation under
196 the right meteorological conditions.
197 To explore the sources of BC and CO, at the RCO, seven-day HYSPLIT back
198 trajectories were run every 6 hours using NCEP/NCAR reanalysis meteorological data
199 (Kalnay et al., 1996). This analysis provided insights on the approximate origin and
200 trajectories of air masses before arriving at RCO measured at the RCO. These
201 HYSPLIT back trajectories were separated into DJF, MAM, JJA, and SON and are shown
202 with MODIS satellite fire count data colored by fire radiative power (FRP, W m^{-2})
203 (Figure 5). The MODIS fire count data and radiative power are used strictly for
204 qualitative, not quantitative, purposes in this work. Here we observe that, as major
205 biomass burning sites moved to the north and west in DJF, transport direction was
206 also primarily northerly, and as biomass burning move to Southern Africa in JJA, the
207 prevailing wind directions were also southerly. Although Rwanda itself had few large-
208 scale fires, its geographical position and meteorology meant that it experienced

transported fire haze from both major burn seasons. Black carbon measured at the station tracked fairly well with summed daily FRP for sub Saharan Africa (Figure 5).

To further examine pollution transport to the RCO, the HYSPLIT back trajectory geographical areas were gridded (using the R Openair package, (Carslaw and Ropkins, 2012)) and merged, using date and time, with measured BC concentrations and mixing ratios of CO to generate concentration-weighted back trajectories (cwt) for each season (more details on cwt available in (Hsu et al., 2003; Seibert et al., 1994))(Figure 6). Trajectory time in each grid and arrival time of each air mass were taken into account in this model to predict the likely source regions and emission concentrations of pollutants measured at the RCO. This was done to determine likely source regions of air pollution at the RCO by comparing arrival times of air masses to the RCO and the time series of pollutants. This method has proven fairly effective at identifying emission sources when comparing predicted emission regions to emissions inventories (Lupu and Maenhaut, 2002) and is good as a rough estimate of emission regions with no apriori information (Kabashnikov et al., 2011). This method has low computational cost and is simple to set up, both of which are important for areas with limited bandwidth or computational capacity and this method can be repeated easily by in-country scientists.

BC and CO appeared to originate from similar areas, as expected due to their overlapping sources of inefficient combustion and biomass burning. During JJA, significant BC and CO appeared to originate from southern Africa and Madagascar, as well as from local sources near the RCO. During DJF, the source of these pollutants appeared to be much closer to the RCO, as major fires in the DRC and Uganda were

232 also closer to the station. Throughout the measurement period, but particularly DJF,
233 the Lake Kivu region also appeared to be a source of BC and CO. The Lake Kivu region
234 is densely populated and use of both cook stoves and diesel generators is common.
235 In addition to direct emissions of BC and CO, other emissions such as volatile
236 organic compounds and oxides of nitrogen from biomass burning are known to affect
237 tropospheric O_3 concentrations, as they are precursors to O_3 formation (Jaffe and
238 Wigder, 2012; Sauvage et al., 2005). It appears that such emissions could have played
239 a role in the observed seasonal increase in O_3 mixing ratios of approximately 20 ppb
240 in DJF and 25 ppb in JJA above rainy season levels at the RCO. This increase of about 5
241 ppb O_3 during JJA versus DJF was potentially due to the mixing of biomass burning
242 emissions with anthropogenic emissions from east African cities such as Nairobi, Dar
243 Es Salam, and Kampala during the JJA dry season. It also could have been the result of
244 generally higher solar radiation during the JJA season in Rwanda (Safari and Gasore,
245 2009). Direct source apportionment of O_3 is difficult as it formed downwind of
246 emissions, but a mix of biomass burning and anthropogenic emissions from southern
247 Africa could have been transported to Rwanda after photochemical aging and
248 processing. During the DJF dry season, fires are closer to Rwanda and away from
249 major urban areas. During June and July, a loose correlation (R=0.47 and 0.45,
250 respectively) between O_3 mixing ratios and BC concentrations was observed, while no
251 correlations (R=-0.04, -0.15, and 0.07) were observed in December, January, and
252 February.

253 **3.2 Absorption Angstrom Exponent and BC Source Apportionment**

It is important to understand the pollution emission sources in East Africa, beyond large-scale biomass burning, in order to enact policies and actions to reduce these emissions. One way scientists have estimated fuel combustion versus biomass burning BC particulate is by measuring the color of the particles (wood smoke particles have enhanced absorption in the UV, while fossil fuel combustion particles have flat absorption over all wavelengths)(Kirchstetter and Thatcher, 2012; Sandradewi et al., 2008). The Aethalometer's seven wavelengths allow measurement of the wavelength-dependent aerosol absorption and the calculation of absorption coefficients that can be used to infer the potential sources of BC aerosol (Drinovec et al., 2015; Sandradewi et al., 2008) measured. Theoretically, from the wavelength dependence of aerosol absorption, BC from fossil fuel and wood smoke can be differentiated(Sandradewi et al., 2008). Though this two-component model can provide a valuable knowledge on knowledge on source attribution of BC this model has some limitations. This model is more accurate if calibrated to local conditions as burning and aging during transport affects aerosol 's wavelength-dependent absorption(Dumka et al., 2013; Harrison et al., 2012), as different fuels and wood biomass burning creates aerosol with different radiative properties and the standard model, based on European studies, has been shown to be less applicable in developing countries (Garg et al., 2016).

From the Aethalometer data, wavelength dependence of absorption coefficients and the absorption Ångstrom exponent (AAE) were calculated and compared to literature values of biomass burning and fossil fuel combustion (Figure 7). The AAE is a dimensionless property commonly used to characterize the

277 wavelength-dependent absorption of BC and gives clues on the source and/or aging of
278 BC when compared to laboratory and other ambient studies(Chung et al., 2012; Lack
279 and Langridge, 2013; Russell et al., 2010; Yuan et al., 2016). The AAE values assigned
280 for the standard Aethalometer model separating the BC from biomass burning and
281 fossil fuel combustion are two and one, respectively (where two represents an
282 average AAE for woodsmoke of different types and ages) (Kirchstetter et al, 2004;
283 Sandradewi et al, 2012; Drinovec et al. 2015). In this work, standard mass absorption
284 cross-sections (MACs) for each wavelength provided by the manufacturer of the
285 Aethalometer were used to calculate the absorption coefficient (b_{abs}) at each
286 wavelength. For pure BC from fossil fuel, $b_{abs} \sim 1/\lambda$ and the AAE between two
287 wavelengths (470 nm and 950 nm) is 1 using the equation $\ln(_{babs}\lambda_1/b_{abs}\lambda_2)/\ln(\lambda_2/\lambda_1)$.
288 The average AAE (averaged for entire measurement period between July 2015
289 and January 2017) was calculated to be 1.65 (+/- 0.14) at the RCO using the 470 and
290 950 wavelength absorption and MACs (Figure 10)(Sandradewi et al., 2008; Drinovec
291 et al. 2015). These wavelengths were chosen as the AAE calculated from 470 and 950
292 is generally comparable with other literature values(Saarikoski et al., 2012). The
293 calculated AAE values were on par with AAE calculated from measurements taken in
294 areas heavily influenced by biomass burning (Chung et al., 2012; Lack and Langridge,
295 2013; Russell et al., 2010; Saleh et al., 2013; Sandradewi et al., 2008; Yuan et al.,
296 2016). Past studies have reported an AAE of 1.2-2.5 for biomass burning
297 aerosol(Andreae and Gelencsér, 2006; Chung et al., 2012; Russell et al., 2010; Saleh et
298 al., 2013, 2014). While daily only small variations (+/- 0.05) for AAE were observed (,
299 significant seasonal differences in this value were found, with monthly averaged

300 values ranging from 1.5 (dry season) to 1.9 (at the end of the long rainy season). This
301 is shown with the 30 day running mean of the AAE (Figure 7). Studies in southern
302 Africa measuring savanna and crop burning found an AAE of around 1.45 for ambient
303 black carbon aerosol, and in the dry season savanna and crop burning are the
304 prevalent type of large-scale biomass burning in sub-Saharan Africa (Russell et al.,
305 2010). The AAE calculated from the Aethalometer data at the RCO was higher during
306 the rainy season when local emissions dominated our measurements (Figure 7).
307 Eucalyptus burning, the most prevalent burning near the station (for charcoal making,
308 cooking fires, brick kiln fuel) was measured in laboratory experiments to have a
309 higher AAE than savanna burning (AAE of 1.71 +/- 0.50 calculated between 405 and
310 781 nm wavelengths)(Chung et al., 2012). Eucalyptus trees and savanna burning were
311 certainly not the only two types of solid biofuel influencing measurements at the
312 station, but the difference in AAE of aerosols produced from different fuels means that
313 the AAE will have large variations based on fuel wood or other biomass used and this
314 was reflected in our data.
315 Using the Aethalometer model with standard inputs not accounting for the
316 different types of fuel used in East Africa versus Europe, a high influence of fossil fuel
317 black carbon emissions was calculated: in the dry season, over 50% of black carbon
318 was assigned to be fossil fuel in origin (Figure 7). Fossil fuel emissions certainly
319 influenced the pollution at the RCO, as air masses from Kigali, Kampala, Nairobi, and
320 Dar es Salaam were transported to the station. These cities have high black carbon
321 emissions from generators, fossil fuel power stations, and older diesel vehicles but
322 would also have significant biomass cook stove emissions (Gatari and Boman, 2003;

323 Koch et al., 2009; Mkoma et al., 2009; van Vliet and Kinney, 2007). However, at <10%
324 fuel demand of fossil fuel (all types, see Table 2) versus >90% wood and charcoal fuel
325 demand, even if the g BC per kg fuel from diesel was 4x higher, and all fossil fuel use
326 was unregulated diesel (unlikely), well under half of the measured BC should be from
327 fossil fuel combustion emissions. Aging with transport would increase the AAE of the
328 aerosol, not decrease, so aging should not cause this seasonal difference as transport
329 distances of BC are longer during the dry seasons.
330 In order to gain more insights into the sources of BC we also examined the
331 BC:CO. CO is also released by inefficient combustion and the ΔBC: ΔCO ratio can be
332 different for different emission sources. In order to calculate this ratio we first
333 converted the CO mixing ratios to concentrations (in $\mu g\ m^{-3}$), and then subtracted the
334 95th percentile values for CO and BC from their respective concentrations. For the
335 entire data set, the ΔBC: ΔCO (both in $\mu g\ m^{-3}$) ratio was 0.014 (R^2 0.79, n = 40523).
336 The ΔBC: ΔCO ratio varied seasonally, with monthly average peaks reaching 0.016 in
337 December, February, and July and lows below 0.01 in April. The average ratio of 0.014
338 for the measurement period was almost twice as high as in biomass burning plumes
339 sampled over West Africa in an aircraft campaign (0.0072)(Moosmüller and
340 Chakrabarty, 2011) but on par with or lower than measurements taken during the
341 INDOEX campaign in the Indian Ocean (Dickerson et al., 2002). A study in Germany
342 and Mexico found a correlation between diesel vehicle use and higher BC:CO
343 (Baumgardner et al., 2002), while other studies have also found an increased
344 ΔBC: ΔCO during periods more influenced by biomass burning (Pan et al., 2011). A
345 study in India found no correlation in biomass-burning and fossil fuel-influenced

346 ΔBC:ΔCO air masses (Sahu et al., 2012), as there are a wide range of ratios measured
347 from the same source (Dickerson et al., 2002; Sahu et al., 2012). The high ΔBC:ΔCO
348 ratio at the RCO could be due to the prevalence of older diesel engines in the country,
349 which emit more BC to CO than newer engines (Cai et al., 2013), but, as the highest
350 value occurs during the Rwanda dry seasons and the continental biomass burning
351 seasons , likely the ratio is governed in part by rainout as BC is more easily removed
352 by wet deposition than CO. In this study, we were not able to use this ratio to further
353 separate biomass burning BC from fossil fuel combustion BC.

354 **3.3 Examination of Local and Regional Pollution**

355 The continuous collection of BC, CO and O_3 data during the dry and rainy
356 seasons allowed examination of both transported and local pollution. Here we define
357 local pollution as pollution originating within twelve hours transport time under
358 typical wind speed conditions (<150 km, including both Rwanda and the border areas
359 with DRC and Uganda). During Rwanda's rainy seasons, the continental fire count is
360 also at a minimum, reducing large-scale biomass burning influence. The region's
361 emissions are from small-scale agricultural burning, charcoal making, cooking fires,
362 brick production (located in the valley below the station and throughout the region),
363 vehicles, diesel and heavy fuel-oil power plants, and diesel generators. These activities
364 continued throughout the rainy season and dry season at similar rates.

365 The baseline daily average BC concentration in the rainy season remained at
366 0.5-1 $\mu g\ m^{-3}$ after 12 hour periods without rain, which could be considered as
367 contributions of small but numerous diffuse emission sources to daily BC
368 concentration in this region. These values, while significantly below those during the

biomass burning affected seasons, are not negligible. If all BC during the rainy seasons is assumed to be local in origin (within one day of transport, as typically rain occurs each day during the rainy season), and this level remained the same throughout the year, yearly average contribution of local emissions to BC would vary between 18-100% of the total measured BC concentration at the RCO. The shoulder months of September and February have been removed from this calculation as they have both rain and biomass burning influence, but on a yearly scale, around 35% of BC concentration measured at the station could originate from local emissions. This is a high estimate as transport of BC is still possible above the boundary layer, but it is on par with previous estimates of the contribution of savanna and forest burning BC emissions versus other emission sources (Bond et al., 2013). While transported savanna, woodland, and forest fire emissions appear to have a huge effect on Rwanda's air quality, targeting local emissions could bring a measurable decrease in PM exposure of the population.

3.3.1 Diurnal Variations in BC, CO and O_3

Diurnal variations in concentration of pollutants can provide important insights into information on local as well as regional pollution emission sources. Diurnal variations in BC concentrations, CO mixing ratios and O_3 mixing ratios observed at RCO in different seasons are shown in Figure 8. At the RCO, the O_3 mixing ratio exhibited a diurnal cycle with a peak in concentration in the evenings, steady levels through the night and a minimum during mid-day. The increase of O_3 in the evening is likely mainly regional O_3 transported above the boundary layer measured at night (as the boundary layer height lowered), but some more locally formed O_3

could also be transported to the station. Similar diurnal O_3 profiles were found at other mountain locations remote from urban centers (Zhang et al., 2015). This diurnal pattern persists in all seasons (Figure 8) and occurred on daily time scales. The differences in diurnal minima and maxima were highest in the June-August period, and lowest in the December-February period. This difference may be due to the differences in biomass burning proximity (far in JJA, closer in DJF), primary wind direction (southerly versus northerly), and also solar intensity (highest in JJA, (Safari and Gasore, 2009)).

BC had mid-morning and early evening peaks that coincided with both cooking times and kerosene/generator use times and with lower boundary layer height in the mornings and evenings. Like with O_3, changing boundary layer conditions also played a role in variations in BC concentrations over the day, as local boundary layer height increased during the day and decreased during the evening and morning hours, and the RCO altitude was above the boundary layer height often during the evening. These peaks persisted throughout the rainy and dry seasons, indicating some influence of local sources for these diurnal peaks as regional transport of BC higher in the atmosphere should be greater in JJA/DJF (more BC) and solely boundary-layer driven BC concentration changes would be greater during these times.. CO mixing ratios had a similar but less pronounced diurnal variation.

3.3.2 Case Study: High and Low Periods of Black Carbon

Seasonal variations are too long to fully capture local pollution events. To further examine local pollution, high BC time periods during DJF and JJA period, and one period of low black carbon in the MAM period, were examined for their BC:CO

ratio and correlation, relationship of O_3 to CO, and AAE (Figure 9). From this figure, no clear trends are observed. The BC:CO is 10 with an R^2 of 0.48 for the polluted DJF period, 8 with an R^2 of 0.47 for non-polluted period in May, and 16.6 with an R^2 of 0.72 for the polluted JJA period. The average AAE for the May period was 1.79, for February 1.53, and for August 1.53 as well. Unfortunately, no O_3 data was available for the August period. O_3 in February was loosely correlated with CO (R^2 0.17) and averaged 39 ppbv, with a peak value of 43. O_3 in May had averaged 26 ppbb with a peak of 34 ppbv, and no correlation with CO.

During the May period, spikes in very local pollution can be seen (Figure 10). These hour plus increases in BC happen at regular cooking times in the valley and, due to their shorter (hourly) time scales of rise and fall, cannot be explained by changes in boundary layer conditions. The diurnal patterns of increased BC during cooking times persist during the polluted period, but on a baseline of regional pollution. Some of the diurnal variability in black carbon background can be attributed to boundary layer conditions, seen with the slow and steady changes over the course of the day not confined to the timescales of activity in the valley.

3.3.3 Comparison to Global and Eastern Africa Measurements

Daily averages of BC at the station often exceeded 5 $\mu g\ m^{-3}$, and the yearly average BC measured at the station was greater than many rural measurement locations around the globe and on-par with urban measurements in North America and Europe, though much lower than measurements made in cities in China (Figure 11). While data from other countries is from multiple years and stations, this does

437 give context to the Rwanda measurements globally. However, more relevant
438 comparisons would be with other areas in Eastern Africa.
439 Recently the US Embassies in Addis Ababa, Ethiopia, and Kampala, Uganda
440 have begun continuously measuring PM2.5 concentrations. The raw data is collected
441 and reported online on the OpenAQ platform (OpenAQ.org). This dataset on PM2.5
442 concentrations in major cities over different seasons in this region has been valuable
443 in gaining basic insights into the seasonal characteristics of PM2.5 concentrations in
444 the region (Figure 12). The PM2.5 concentrations in both these cities showed clear
445 seasonal patterns, though the seasonal patterns differed at the two sites. Addis Ababa
446 (Ethiopia) is much further north than Rwanda and Ethiopia is in general higher in
447 elevation than Rwanda (though at 2355 m, not higher than the RCO) and closer to the
448 Indian Ocean. In Addis Ababa, the dry season is also in DJF, but measured PM2.5
449 concentrations were low during this season. HYSPLIT back trajectory calculations
450 confirmed that air masses during this time of the year originated over the ocean, not
451 from the continent. Kampala, Uganda is close to Rwanda, near the equator, and has a
452 long dry season during JJA and a short dry season during DJF. Rainy and dry season
453 extrema are shown in the available Kampala PM2.5 data, with an enhancement during
454 February and JJA of around 15 to 25-30 $\mu g\ m^{-3}$, respectively, above PM2.5
455 concentrations during other months. However, in Kampala during all months
456 measured, including the rainy season where little regional biomass burning influence
457 is likely, monthly averages remained above the WHO recommendations for air
458 pollution levels at daily averages of 25 $\mu g\ m^{-3}$ or less and, despite having a lower
459 population than Addis, were consistently higher in PM2.5 concentrations. South Africa

460 has the most air quality monitoring stations of any sub-Saharan African country and
461 results from these stations show a PM2.5 peak only in the southern burning season
462 (JJA), not surprisingly missing transported pollution from the northern (DJF) burning
463 season (Hersey et al., 2015). From these data, though there are only two data points,
464 it appears that African countries near the equator may be positioned to experience six
465 months per year of transported regional fire haze, from both the northern and
466 southern biomass burning seasons.

467 Beyond BC and PM3.5, the MOZAIC campaign in the late 1990s and early 2000s
468 measured ambient O_3 mixing ratios at the Nairobi, Kampala, and Kigali airports . This
469 campaign found Kigali, despite its smaller size and lower vehicle count, to have the
470 highest O_3 mixing ratios among them (Sauvage et al., 2005). They measured a similar
471 in magnitude increase in surface O_3 mixing ratios during the JJA season in Rwanda as
472 our measurements at the RCO, although DJF was not measured in their work. O3
473 measurements were made in Brazzaville, Republic of the Congo during January and
474 February O_3. While much further west than Rwanda, in Brazzaville O_3 mixing ratios
475 also increased during January and February, parallel to Rwanda, with monthly
476 averages during January and February 25 ppb greater than the minimum of <30 ppb
477 in April (Sauvage et al., 2005). This suggests influence from northern hemisphere
478 biomass burning to O_3 mixing ratios at Brazzaville. O_3 in JJA at Brazzaville was almost
479 30 ppb higher than in January and February, however, so transport of air mass from
480 the south and southern Africa biomass burning had a greater influence on O_3 in the
481 region than transport from the north and biomass burning in central Africa. The 1992
482 SAFARI campaign also measured O_3 in sub-Saharan Africa throughout all seasons, and

483 measured a seasonal ozone concentration peak during the JJA period for central and
484 southern Africa (Thompson et al., 1996). A separate, large peak for DJF was not as
485 observable in the SAFARI data (Thompson et al., 1996). SAFARI measurements took
486 place prior to 1993, meaning that significant development in sub-Saharan Africa could
487 have taken place between the SAFARI campaign and the MOZAIC campaign (1997-
488 2003) that could drive the increasing O_3 in DJF as well as JJA over a period of almost a
489 decade. The SAFARI campaign measured the total column O_3, not the ground-level O_3
490 mixing ratios, so data are not directly comparable.

491 **4. Conclusions**

492 In this work, we present the first long-term and continuous measurements of
493 short-lived climate forcers for a nearly two-year period from July 2015 to January
494 2017 at the Rwanda Climate Observatory located at Mt. Mugogo in Rwanda. From
495 these observations, we find that:

496 1. During Rwanda's two dry seasons, transported pollution led to high
497 black carbon and carbon monoxide levels at the RCO, surpassing
498 concentrations measured in many major cities elsewhere. Emissions
499 from large-scale crop and savanna fires appeared to have a wide-
500 reaching effect on this region, reflected in increased PM2.5 in
501 Kampala, a major East African city, for both biomass burning seasons
502 and likely driving the increased O_3 measured during DJF and JJA by
503 our study and by past studies in equatorial Africa. The dense
504 population of equatorial East Africa and the double impact of the two
505 fires seasons could lead to significant public health problems for the

population in Rwanda and equatorial East Africa as exposure to elevated levels of PM2.5 and BC concentrations occurs six months out of the year.

2. Ground level O_3 was enhanced during both dry seasons, likely due to the prevalent wide-scale biomass burning. Increased enhancement was observed during the JJA dry season when solar intensity was higher and the air masses originated from the southeast and likely included a mix of biomass burning and anthropogenic emissions (cooking fires, vehicles, industries). As this area develops and population grows, local as well as regional air pollution could become a major environmental and societal issue that could be a threat to national development goals.

3. Local emissions beyond large-scale biomass burning influence were constant and estimated to contribute up to 35% of the annual average measured black carbon concentration, if black carbon during the rainy season was assumed to be completely local (Rwanda and neighboring countries) in origin (ranging from 0.5-1 $\mu g\ m^{-3}$ daily average measured BC). These local emissions, from different combustion sources (e.g., cooking fires, inefficient diesel generators and engines with sub-standard fuel use, solid biomass fuel burning, small agricultural fires), are likely concentrated in the densely populated Rwanda and Lake Kivu economic area. Rwanda's population is growing quickly and, as these local emissions are

related to population density, air pollution will likely increase unless there is government intervention.

4. Different combustion fuel and burning practices in Europe and East Africa calls into question the accuracy and applicability of a two-component model for estimating BC from fossil fuel combustion and biomass burning using AAE approximations for biomass burning and fossil fuel combustion aerosol measured in Europe for use in East Africa. There may also be different mass absorption cross-sections for aerosols measured at the RCO than in Europe or North America. This shows the need for multiple on-ground measurements to fully understand pollution sources in different regions of the world, notably in Africa. However, seasonal variations in the wavelength dependence of ambient BC particles did point to different sources of BC particles and this should be further explored in future studies.

5. The measurements we have provided in this study will be useful in advancing atmospheric science in Africa, improve emission inventories and air pollution/atmospheric models in the region, and designing mitigation measures in the region, which has limited long-term and in-situ atmospheric data.

These data and analyses, while acknowledging the high influence of regional biomass burning, also show that measurable decreases in air pollution could be achieved within eastern and central Africa with targeted local policies, emphasizing

cleaner diesel vehicles and generators, reduced wood-fuel reliance for cook stoves, and improved cook stoves to burn biomass fuel more efficiently. Currently, over 2 million households in Rwanda rely on wood burning (including charcoal) for cooking. While reducing this number will have significant economic costs, putting in place infrastructure for alternative cooking fuels (pellet stoves, LPG stoves, electrical stoves) could help the country avoid even higher local air pollution emissions and associated adverse impacts as the population grows. Diesel-fueled minibuses, common transport between towns in Rwanda and within Kigali, and older diesel vehicles are also high emitters of black carbon but newer vehicles with emissions control technology may be economically beyond the reach of local bus companies and citizens. Continuing to grow electrical capacity and connection will reduce the use of kerosene lanterns and diesel generators, and will reduce air pollution if additional energy capacity is achieved through renewable sources (solar, hydropower). The huge influence of regional biomass burning, exacerbated by equatorial East Africa's meteorology, and the potential influence of anthropogenic emissions from major cities on O_3 formation in this regions must also be examined as this area develops. Halting slash-and-burn agriculture, reducing trash incineration, and developing ways to warn the population during periods of high pollution from naturally occurring savanna and forest fires should be an important agenda for regional discussions on environmental, public health, and other development issues.

6. Future Work

The government of Rwanda is working to establish an air quality and climate change monitoring network throughout the country to measure ambient criteria air

pollutants and other key climate change related components of atmospheric pollution. Building knowledge of air quality and climate change related emissions in this data-poor area of the world is essential to fill the large data and knowledge gap in this region. Adding ground-based measurements, comparing measurements to satellite data, using data to evaluate and improve existing emission inventories, improving accuracy of global/regional air quality and climate change models, and using data for quantification of impacts of air pollution and climate change will help local governments design appropriate mitigation strategies rooted in data and local context.

7. Data Availability

This data will be made available at the AGAGE website, https://agage.mit.edu/data/agage-data. All data used in this article will be made available as of publication and data from this project on a rolling basis after quality control.

Acknowledgments:

We thank the generous MIT alumni donors to the MIT-Rwanda Climate Observatory Project that provided the funds to purchase, develop and install most of the instruments at the Rwanda Climate Observatory. Additional funds for this purpose were provided by the MIT Center for Global Change Science. COMESA provided the funds to purchase and install the Aethalometer at the RCO. We also thank the Government of Rwanda and the Rwanda Ministry of Education, specifically Mike Hughes, Vianney Rugamba, and Dr. Marie Christine Gasingirwa, for supporting this project, including funding the staffing and infrastructure costs of the Rwanda Climate

598 Observatory and the University of Rwanda for providing laboratory space and
599 infrastructure for instrument testing. We thank Dr. Arnico Panday who provided
600 guidance during the initial stages of this project. We also wish to acknowledge the
601 essential contributions of the Mugogo station technical experts Theobard Habineza,
602 Modeste Mugabo, Olivier Shyaka, and Gaston Munyampundu, and RBA technician
603 Yves Fidele, without which running this station would be impossible.
604
605

606 Table 1: Instruments used in this study and measurement period used for analysis

INSTRUMENT	SPECIES MEASURED	MEASUREMENT PERIOD	TIME RESOLUTION
PICARRO G2401 CAVITY RING DOWN SPECTROMETER	CO_2, CO, CH_4, H_2O	MAY 2015-JANUARY 2017	1 MIN
MAGEE SCIENTIFIC AE33 7-WAVELENGTH AETHALOMETER	BLACK CARBON (PM2.5, CYCLONE IMPACTOR ON INLET)	MAY 2015-JANUARY 2017	1 MIN
TELEDYNE T400 API	O_3	MAY 2015-JANUARY 2017	1 MIN
VAISALA WXT	MET PARAMETERS (RH, WS, WD, T, P)	JULY 2015-JANUARY 2017	1S

Table 2:

Fuel Demand in Rwanda (2016, Rwanda Ministry of Infrastructure)

Fuel Type	Demand
Petrol	120442 kL
Diesel	178529 kL
Kerosene	22288 kL
Heavy Fuel Oils	59292 kL
Jet-A	18235 kL
Wood (charcoal + natural)	4,200,000 metric tons

613 References
614
615 Andreae, M. O. and Gelencsér, A.: Black carbon or brown carbon? The nature of light-
616 absorbing carbonaceous aerosols, Atmos. Chem. Phys., 6(3), 3419–3463,
617 doi:10.5194/acpd-6-3419-2006, 2006.
618 Archibald, S., Nickless, A., Govender, N., RJ., S. and Lehsten, V.: Climate and the inter-
619 annual variability of fire in southern Africa: a meta-analysis using long-term field data
620 and satellite-derived burnt area data, Glob. Ecol. Biogeogr., 19(6), 794–809, 2010.
621 Baumgardner, D., Raga, G., Peralta, O., Rosas, I., Castro, T., Kuhlbusch, T., John, A. and
622 Petzold, A.: Diagnosing black carbon trends in large urban areas using carbon
623 monoxide measurements, J. Geophys. Res. Atmos., 107(21),
624 doi:10.1029/2001JD000626, 2002.
625 Bond, T. C., Doherty, S. J., Fahey, D. W., Forster, P. M., Berntsen, T., DeAngelo, B. J.,
626 Flanner, M. G., Ghan, S., Kärcher, B., Koch, D., Kinne, S., Kondo, Y., Quinn, P. K., Sarofim,
627 M. C., Schultz, M. G., Schulz, M., Venkataraman, C., Zhang, H., Zhang, S., Bellouin, N.,
628 Guttikunda, S. K., Hopke, P. K., Jacobson, M. Z., Kaiser, J. W., Klimont, Z., Lohmann, U.,
629 Schwarz, J. P., Shindell, D., Storelvmo, T., Warren, S. G. and Zender, C. S.: Bounding the
630 role of black carbon in the climate system: A scientific assessment, J. Geophys. Res.
631 Atmos., 118(11), 5380–5552, doi:10.1002/jgrd.50171, 2013.
632 Cai, H., Burnham, A. and Wang, M.: Updated Emission Factors of Air Pollutants from
633 Vehicle Operations in GREET TM Using MOVES, , (September), 2013.
634 Carslaw, D. C. . and Ropkins, K.: The openair manual open-source tools for analysing
635 air pollution data, King's Coll. London, 27–28(January), 287, 2012.
636 Chung, C. E., Kim, S. W., Lee, M., Yoon, S. C. and Lee, S.: Carbonaceous aerosol AAE
637 inferred from in-situ aerosol measurements at the Gosan ABC super site, and the
638 implications for brown carbon aerosol, Atmos. Chem. Phys., 12(14), 6173–6184,
639 doi:10.5194/acp-12-6173-2012, 2012.
640 Crutzen, P. J. and Andreae, M.: Biomass Burning in the Tropics : Impact on
641 Atmospheric Chemistry and Biogeochemical Cycles Estimates of Worldwide Biomass
642 Burning, Science (80-.)., 250(4988), 1669–1678, doi:10.1126/science.250.4988.1669,
643 1990.
644 Dickerson, R. R., Andreae, M. O., Campos, T., Mayol-Bracero, O. L., Neususess, C. and
645 Streets, D. G.: Analysis of black carbon and carbon monoxide observed over the Indian
646 Ocean: Implications for emissions and photochemistry, J. Geophys. Res., 107(D19),
647 doi:Artn 8017\rDoi 10.1029/2001jd000501, 2002.
648 Drinovec, L., Močnik, G., Zotter, P., Prévôt, A. S. H., Ruckstuhl, C., Coz, E., Rupakheti, M.,
649 Sciare, J., Müller, T., Wiedensohler, A. and Hansen, A. D. A.: The "dual-spot"
650 Aethalometer: An improved measurement of aerosol black carbon with real-time
651 loading compensation, Atmos. Meas. Tech., 8(5), 1965–1979, doi:10.5194/amt-8-
652 1965-2015, 2015.
653 Dumka, U. C., Manchanda, R. K., Sinha, P. R., Sreenivasan, S., Moorthy, K. K. and Suresh
654 Babu, S.: Temporal variability and radiative impact of black carbon aerosol over
655 tropical urban station Hyderabad, J. Atmos. Solar-Terrestrial Phys., 105–106(April
656 2016), 81–90, doi:10.1016/j.jastp.2013.08.003, 2013.
657 Field, R. D., van der Werf, G. R., Fanin, T., Fetzer, E. J., Fuller, R., Jethva, H., Levy, R.,
658 Livesey, N. J., Luo, M., Torres, O. and Worden, H. M.: Indonesian fire activity and smoke

659 pollution in 2015 show persistent nonlinear sensitivity to El Niño-induced drought,
660 Proc. Natl. Acad. Sci., 113(33), 9204–9209, doi:10.1073/pnas.1524888113, 2016.
661 Garg, S., Chandra, B. P., Sinha, V., Sarda-Esteve, R., Gros, V. and Sinha, B.: Limitation of
662 the Use of the Absorption Angstrom Exponent for Source Apportionment of
663 Equivalent Black Carbon: a Case Study from the North West Indo-Gangetic Plain,
664 Environ. Sci. Technol., 50(2), 814–824, doi:10.1021/acs.est.5b03868, 2016.
665 Gasore, J.: Quantifying Emissions of Carbon Dioxide and Methane in Central and
666 Eastern Africa Through High Frequency Measurements and Inverse Modeling,
667 Massachusetts Institute of Technology., 2018.
668 Gatari, M. J. and Boman, J.: Black carbon and total carbon measurements at urban and
669 rural sites in Kenya, East Africa, Atmos. Environ., 37(8), 1149–1154,
670 doi:10.1016/S1352-2310(02)01001-4, 2003.
671 Harrison, R. M., Beddows, D. C. S., Hu, L. and Yin, J.: Comparison of methods for
672 evaluation of wood smoke and estimation of UK ambient concentrations, Atmos.
673 Chem. Phys., 12(17), 8271–8283, doi:10.5194/acp-12-8271-2012, 2012.
674 Hersey, S. P., Garland, R. M., Crosbie, E., Shingler, T., Sorooshian, A., Piketh, S. and
675 Burger, R.: An overview of regional and local characteristics of aerosols in South
676 Africa using satellite, ground, and modeling data, Atmos. Chem. Phys., 15(8), 4259–
677 4278, doi:10.5194/acp-15-4259-2015, 2015.
678 Hsu, Y. K., Holsen, T. M. and Hopke, P. K.: Comparison of hybrid receptor models to
679 locate PCB sources in Chicago, Atmos. Environ., 37(4), 545–562, doi:10.1016/S1352-
680 2310(02)00886-5, 2003.
681 Kabashnikov, V. P., Chaikovsky, A. P., Kucsera, T. L. and Metelskaya, N. S.: Estimated
682 accuracy of three common trajectory statistical methods, Atmos. Environ., 45(31),
683 5425–5430, doi:10.1016/j.atmosenv.2011.07.006, 2011.
684 Kalnay, E., Kanamitsu, M., Kistler, R., Collins, W., Deaven, D., Gandin, L., Iredell, M.,
685 Saha, S., White, G., Woollen, J., Zhu, Y., Chelliah, M., Ebisuzaki, W., Higgins, W.,
686 Janowiak, J., Mo, K. C., Ropelewski, C., Wang, J., Leetmaa, A., Reynolds, R., Jenne, R. and
687 Joseph, D.: The NCEP/NCAR 40-year reanalysis project, Bull. Am. Meteorol. Soc., 77(3),
688 437–471, doi:10.1175/1520-0477(1996)077<0437:TNYRP>2.0.CO;2, 1996.
689 Kirchstetter, T. W. and Thatcher, T. L.: Contribution of organic carbon to wood smoke
690 particulate matter absorption of solar radiation, Atmos. Chem. Phys., 12(14), 6067–
691 6072, doi:10.5194/acp-12-6067-2012, 2012.
692 Koch, D., Schulz, M., Kinne, S., McNaughton, C., Spackman, J. R., Balkanski, Y., Bauer, S.,
693 Berntsen, T., Bond, T. C., Boucher, O., Chin, M., Clarke, A., De Luca, N., Dentener, F.,
694 Diehl, T., Dubovik, O., Easter, R., Fahey, D. W., Feichter, J., Fillmore, D., Freitag, S., Ghan,
695 S., Ginoux, P., Gong, S., Horowitz, L., Iversen, T., Kirkevåg, A., Klimont, Z., Kondo,
696 Y., Krol, M., Liu, X., Miller, R., Montanaro, V., Moteki, N., Myhre, G., Penner, J. E.,
697 Perlwitz, J., Pitari, G., Reddy, S., Sahu, L., Sakamoto, H., Schuster, G., Schwarz, J. P.,
698 Seland, Ø., Stier, P., Takegawa, N., Takemura, T., Textor, C., van Aardenne, J. a. and
699 Zhao, Y.: Evaluation of black carbon estimations in global aerosol models, Atmos.
700 Chem. Phys., 9(22), 9001–9026, doi:10.5194/acp-9-9001-2009, 2009.
701 Lack, D. A. and Langridge, J. M.: On the attribution of black and brown carbon light
702 absorption using the aerosol angstrom exponent, Atmos. Chem. Phys., 13(20), 10535–
703 10543, doi:10.5194/acp-13-10535-2013, 2013.
704 Lupu, A. and Maenhaut, W.: Application and comparison of two statistical trajectory

705 techniques for identification of source regions of atmospheric aerosol species, Atmos.
706 Environ., 36(36–37), 5607–5618, doi:10.1016/S1352-2310(02)00697-0, 2002.
707 Mkoma, S. L., Maenhaut, W., Chi, X., Wang, W. and Raes, N.: Characterisation of PM10
708 atmospheric aerosols for the wet season 2005 at two sites in East Africa, Atmos.
709 Environ., 43(3), 631–639, doi:10.1016/j.atmosenv.2008.10.008, 2009.
710 Moosmüller, H. and Chakrabarty, R. K.: Technical Note: Simple analytical relationships
711 between Ångström coefficients of aerosol extinction, scattering, absorption, and single
712 scattering albedo, Atmos. Chem. Phys., 11(20), 10677–10680, doi:10.5194/acp-11-
713 10677-2011, 2011.
714 Niang, I., Ruppel, O. C., Abdrabo, M. A., Essel, A., Lennard, C., Padgham, J. and Urquhart,
715 P.: Africa, Clim. Chang. 2014 Impacts, Adapt. Vulnerability - Contrib. Work. Gr. II to
716 Fifth Assess. Rep. Intergov. Panel Clim. Chang., 1199–1265,
717 doi:10.1017/CBO9781107415386.002, 2014.
718 Pan, X. L., Kanaya, Y., Wang, Z. F., Liu, Y., Pochanart, P., Akimoto, H., Sun, Y. L., Dong, H.
719 B., Li, J., Irie, H. and Takigawa, M.: Correlation of black carbon aerosol and carbon
720 monoxide in the high-altitude environment of Mt. Huang in Eastern China, Atmos.
721 Chem. Phys., 11(18), 9735–9747, doi:10.5194/acp-11-9735-2011, 2011.
722 Prinn, R. G., Weiss, R. F., Fraser, P. J., Simmonds, P. G., Cunnold, D. M., Alyea, F. N.,
723 O'Doherty, S., Salameh, P., Miller, B. R., Huang, J., Wang, R. H. J., Hartley, D. E., Harth, C.,
724 Steele, L. P., Sturrock, G., Midgley, P. M. and McCulloch, A.: A history of chemically and
725 radiatively important gases in air deduced from ALE/GAGE/AGAGE, J. Geophys. Res.
726 Atmos., 105(D14), 17751–17792, doi:10.1029/2000JD900141, 2000.
727 Ramanathan, V. and Carmichael, G.: Global and regional climate changes due to black
728 carbon, Nat. Geosci., 1, 221–227, doi:10.1038/ngeo156, 2008.
729 Real, E., Orlandi, E., Law, K. S., Fierli, F., Josset, D., Cairo, F., Schlager, H., Borrmann, S.,
730 Kunkel, D., Volk, C. M., McQuaid, J. B., Stewart, D. J., Lee, J., Lewis, A. C., Hopkins, J. R.,
731 Ravegnani, F., Ulanovski, A. and Liousse, C.: Cross-hemispheric transport of central
732 African biomass burning pollutants: Implications for downwind ozone production,
733 Atmos. Chem. Phys., 10(6), 3027–3046, doi:10.5194/acpd-9-17385-2009, 2010.
734 Russell, P. B., Bergstrom, R. W., Shinozuka, Y., Clarke, a. D., DeCarlo, P. F., Jimenez, J. L.,
735 Livingston, J. M., Redemann, J., Holben, B., Dubovik, O. and Strawa, A.: Absorption
736 Angstrom Exponent in AERONET and related data as an indicator of aerosol
737 composition, Atmos. Chem. Phys., 10, 1156–1169, doi:10.5194/acpd-9-21785-2009,
738 2010.
739 Saarikoski, S., Carbone, S., Decesari, S., Giulianelli, L., Angelini, F., Canagaratna, M., Ng,
740 N. L., Trimborn, a., Facchini, M. C., Fuzzi, S., Hillamo, R. and Worsnop, D.: Chemical
741 characterization of springtime submicrometer aerosol in Po Valley, Italy, Atmos.
742 Chem. Phys., 12(18), 8401–8421, doi:10.5194/acp-12-8401-2012, 2012.
743 Safari, B. K. (University of R. and Gasore, J. (University of R.: Estimation of Global Solar
744 Radiation in Rwanda Using Empirical Models, Asian J. Sci. Res., 2(2), 68–75,
745 doi:10.3923/ajsr.2009.68.75, 2009.
746 Sahu, L. K., Kondo, Y., Moteki, N., Takegawa, N., Zhao, Y., Cubison, M. J., Jimenez, J. L.,
747 Vay, S., Diskin, G. S., Wisthaler, A., Mikoviny, T., Huey, L. G., Weinheimer, A. J. and
748 Knapp, D. J.: Emission characteristics of black carbon in anthropogenic and biomass
749 burning plumes over California during ARCTAS-CARB 2008, J. Geophys. Res. Atmos.,
750 117(16), 1–20, doi:10.1029/2011JD017401, 2012.

751 Saleh, R., Hennigan, C. J., McMeeking, G. R., Chuang, W. K., Robinson, E. S., Coe, H.,
752 Donahue, N. M. and Robinson, A. L.: Absorptivity of brown carbon in fresh and photo-
753 chemically aged biomass-burning emissions, Atmos. Chem. Phys., 13(15), 7683–7693,
754 doi:10.5194/acp-13-7683-2013, 2013.
755 Saleh, R., Robinson, E. S., Tkacik, D. S., Ahern, A. T., Liu, S., Aiken, A. C., Sullivan, R. C.,
756 Presto, A. a., Dubey, M. K., Yokelson, R. J., Donahue, N. M. and Robinson, A. L.:
757 Brownness of organics in aerosols from biomass burning linked to their black carbon
758 content, Nat. Geosci., 7(September), 1–4, doi:10.1038/ngeo2220, 2014.
759 Sandradewi, J., Prévôt, A. S. H., Szidat, S., Perron, N., Alfarra, M. R., Lanz, V. A.,
760 Weingartner, E. and Baltensperger, U.: Using Aerosol Light Absorption Measurements
761 for the Quantitative Determination of Wood Burning and Traffic Emission
762 Contributions to Particulate Matter, Environ. Sci. Technol., 42(9), 3316–3323,
763 doi:10.1021/es702253m, 2008.
764 Sauvage, B., Thouret, V., Cammas, J. P., Gheusi, F., Athier, G. and Nédélec, P.:
765 Tropospheric ozone over Equatorial Africa: regional aspects from the MOZAIC data,
766 Atmos. Chem. Phys., 5, 311–335, doi:10.5194/acpd-4-3285-2004, 2005.
767 Seibert, P., Kromp-Kolb, H., Baltensperger, U., Jost, D. T. and Schwikowski, M.:
768 Trajectory Analysis of High-Alpine Air Pollution Data, in Air Pollution Modeling and
769 Its Application: NATO: Challenges of Modern Society, edited by S.-E. (Riso N. L.
770 Gryning and M. M. (Centre for E. S. of the M. Millan, pp. 595–596, Springer USA., 1994.
771 Thompson, A. M., Diab, R. D., Bodeker, G. E., Zunckel, M., Coetzee, G. J. R., Archer, C. B.,
772 Mcnamara, D. P., Pickering, K. E., Combrink, J., Fishman, J. and Nganga, D.: Ozone over
773 southern Africa during SAFARI-92 / TRACE A, , 101(95), 1996.
774 van Vliet, E. D. S. and Kinney, P. L.: Impacts of roadway emissions on urban particulate
775 matter concentrations in sub-Saharan Africa: new evidence from Nairobi, Kenya,
776 Environ. Res. Lett., 2(4), 45028, doi:10.1088/1748-9326/2/4/045028, 2007.
777 Welp, L. R., Keeling, R. F., Weiss, R. F., Paplawsky, W. and Heckman, S.: Design and
778 performance of a Nafion dryer for continuous operation at CO2and CH4 air
779 monitoring sites, Atmos. Meas. Tech., 6(5), 1217–1226, doi:10.5194/amt-6-1217-
780 2013, 2013.
781 WHO: Health Effects of Particulate Matter: Policy imlications for countries in eastern
782 Europe, Caucasus and central Asia, World Heal. Organ., 15 [online] Available from:
783 www.euro.who.int, 2013.
784 Yuan, J. F., Huang, X. F., Cao, L. M., Cui, J., Zhu, Q., Huang, C. N., Lan, Z. J. and He, L. Y.:
785 Light absorption of brown carbon aerosol in the PRD region of China, Atmos. Chem.
786 Phys., 16(3), 1433–1443, doi:10.5194/acp-16-1433-2016, 2016.
787 Zhang, L., Jin, L., Zhao, T., Yin, Y., Zhu, B., Shan, Y., Guo, X., Tan, C., Gao, J. and Wang, H.:
788 Diurnal variation of surface ozone in mountainous areas: Case study of Mt. Huang,
789 East China, Sci. Total Environ., 538, 583–590, doi:10.1016/j.scitotenv.2015.08.096,
790 2015.
791
792

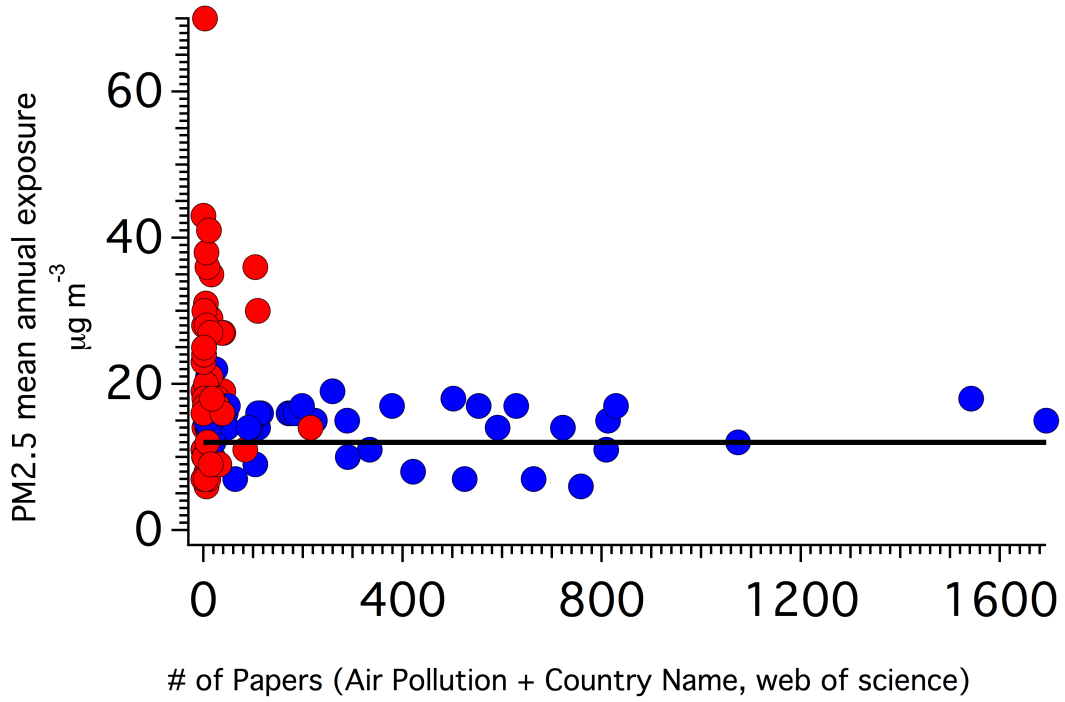

Figure 1: Africa (red) and Europe (blue), PM2.5 mean annual exposure (https://data.worldbank.org/indicator/en.atm.pm25.mc.m3) and paper count of country + air pollution.

809
810

811 **Figure 2**. From top left moving counter-clockwise: an aerial view of RCO at Mt.

812 Mugogo Main Peak, the station with towers in the background, and the location of Mt.

813 Mugogo in Rwanda (blue pin) in relation to Kigali (yellow pin).

814

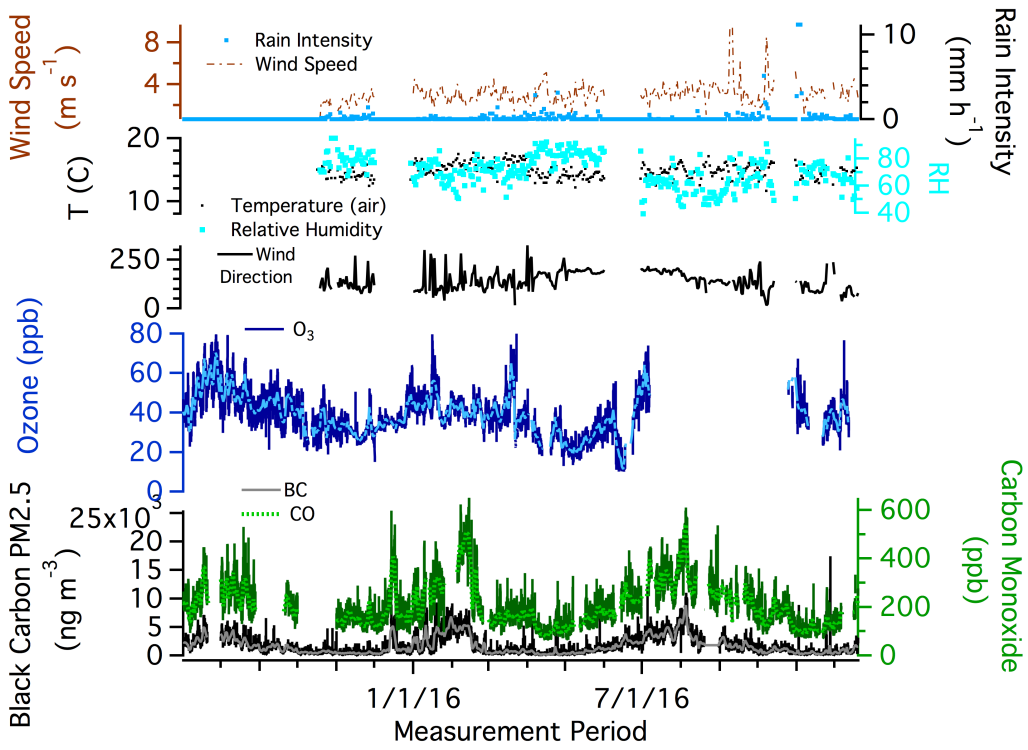

815

816

817 **Figure 3**. From the top down up: (a) wind speed (red dotted) and rain intensity (blue

818 dash) daily average values; (b) temperature (black) and relative humidity (light blue)

819 values; (c) ozone (dark blue, light blue) (15 minute, daily); (d) black carbon (black,

820 grey) and carbon monoxide (dark green, light green) (15 minute, daily) average

821 concentrations.

822

823
824
825
826
827
828
829
830
831

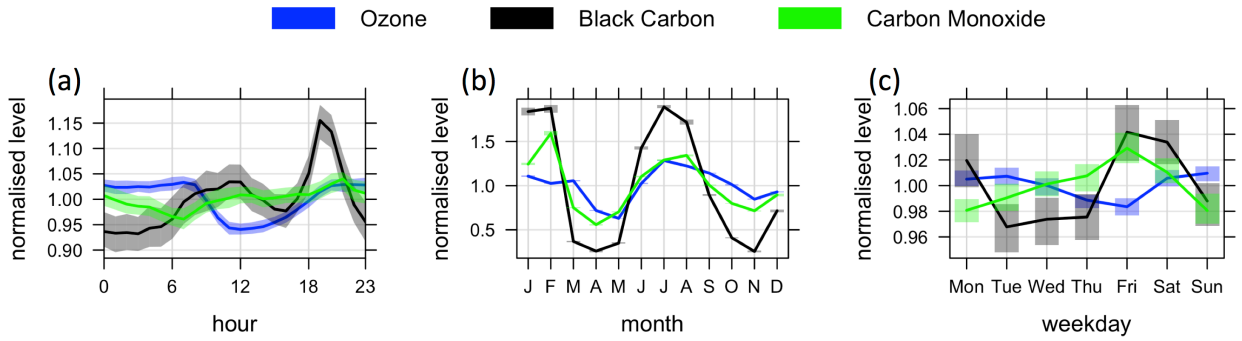

Figure 4. Normalized temporal variations of O_3 mixing ratios, CO mixing ratios, and BC concentrations: (a) diurnal (b) monthly concentrations, and (c) differences by day of the week. Shaded areas are 95% confidence intervals.

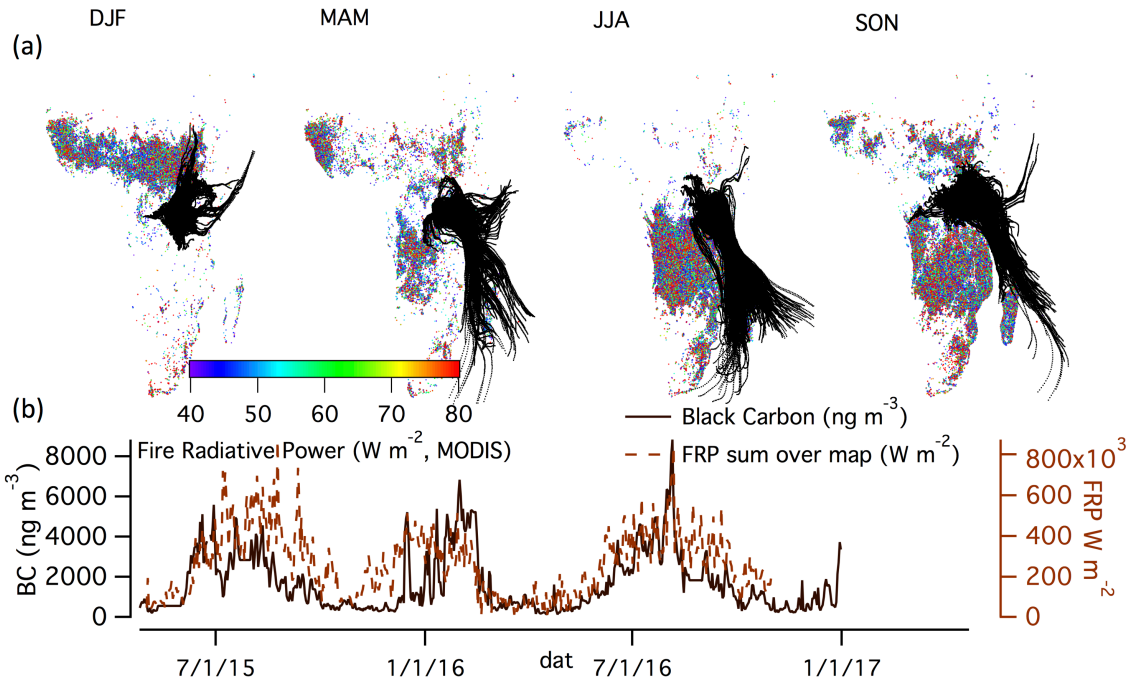

Figure 5. (a) Seasonal fire radiative power data acquired with the MODIS instrument and back trajectories of air masses (generated with the HYSPLIT model) reaching the Rwanda Climate Observatory for the period May 2015 to January 2017. Seasons in Rwanda are split into: short dry season, December-January-February (DJF), long rainy season, March-April-May (MAM), long dry season, June-July-August (JJA,) and short rainy season, September-October-November (SON). (b) The time series of daily average BC concentration and the daily sum of Fire Radiative Power (W m^{-2}) from the pictured data bound by the furthest HYSPLIT backtrajectory reaches each season (box defined by the most north, south, east, and west point the HYSPLIT backtrajectories reach).

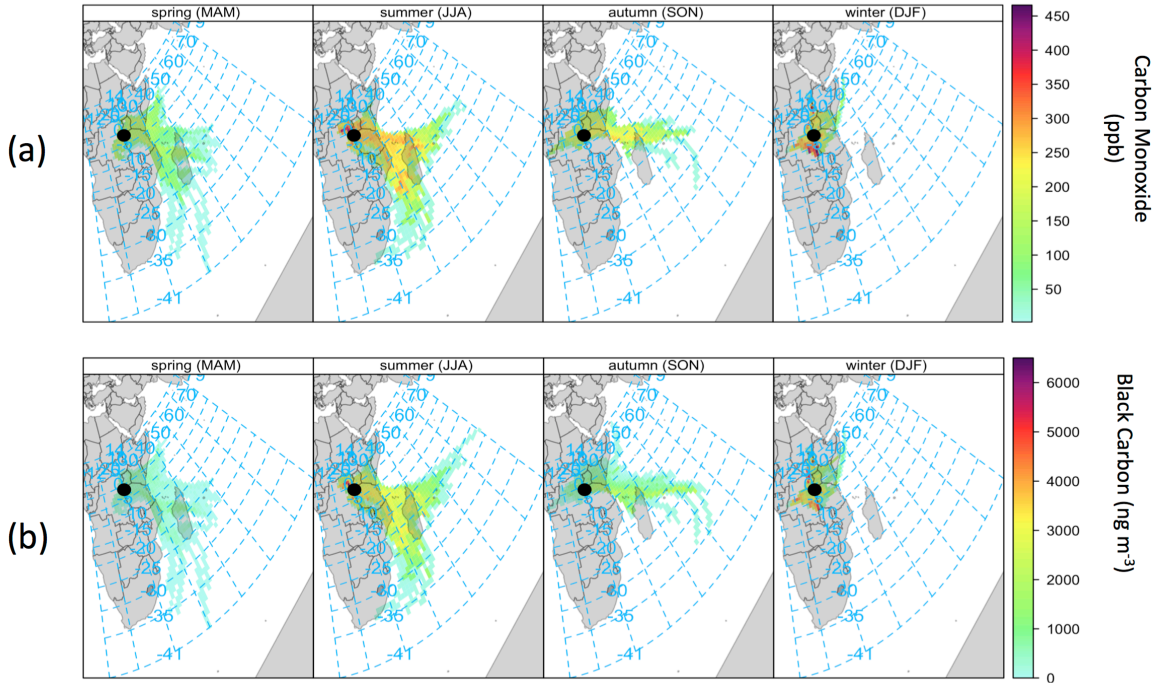

Figure6. Concentration-weighted back trajectories of (a) CO and (b) BC, separated by season, for measurements at the Rwanda Climate Observatory (black dot) for the period of July 2015-January 2017.

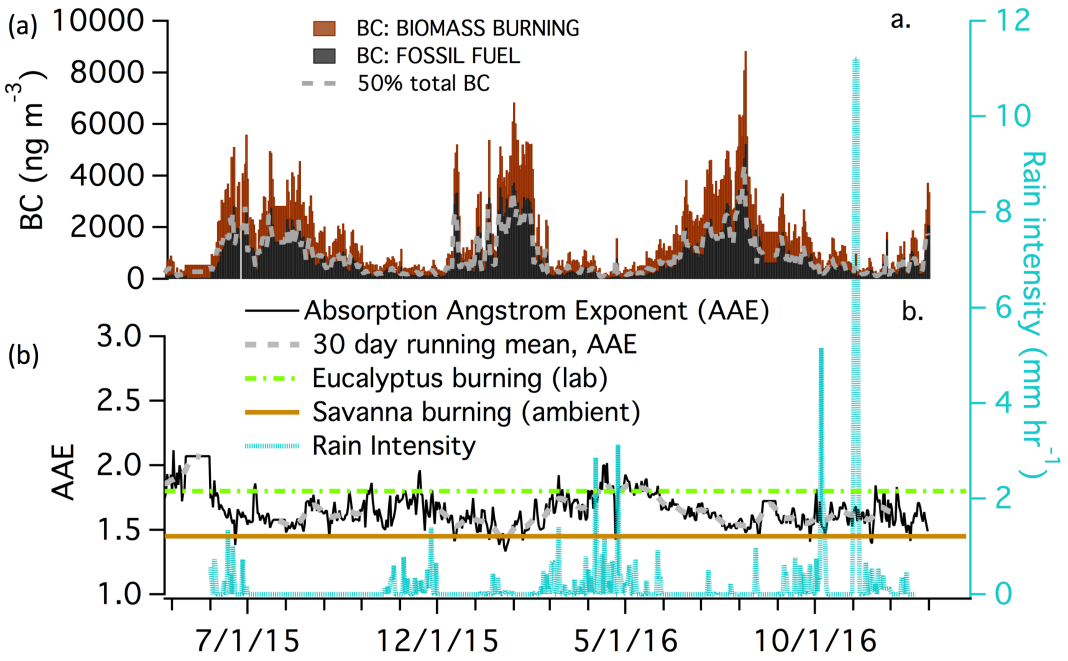

875
876
877

878 **Figure 7**. (a) Time series of contributions of fossil fuel combustion and biomass

879 burning to BC concentrations observed at RCO. (b) Daily average absorption

880 Angstrom exponent (AAE) measured at RCO (black line), rain intensity, and published

881 AAE for Eucalyptus burning ((Yuan et al., 2016), laboratory studies, green line) and

882 savanna burning ((Russell et al., 2010), ambient, brown line) also shown as reference.

883

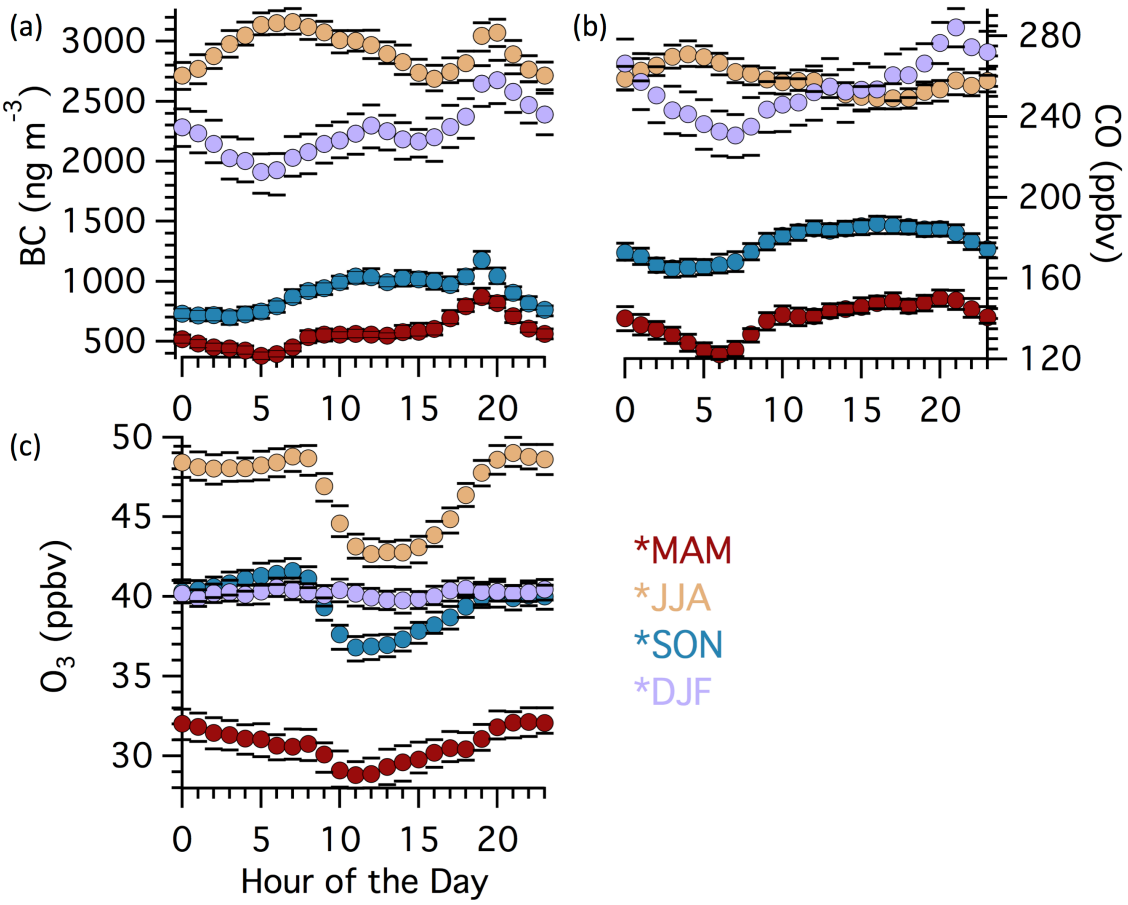

Figure 8. Seasonally separated diurnal profiles of (a) BC concentrations, (b) CO mixing ratios, and (c) O_3 mixing ratios, colored for each season. The circles represent mean concentrations and the lines represent 95% confidence intervals.

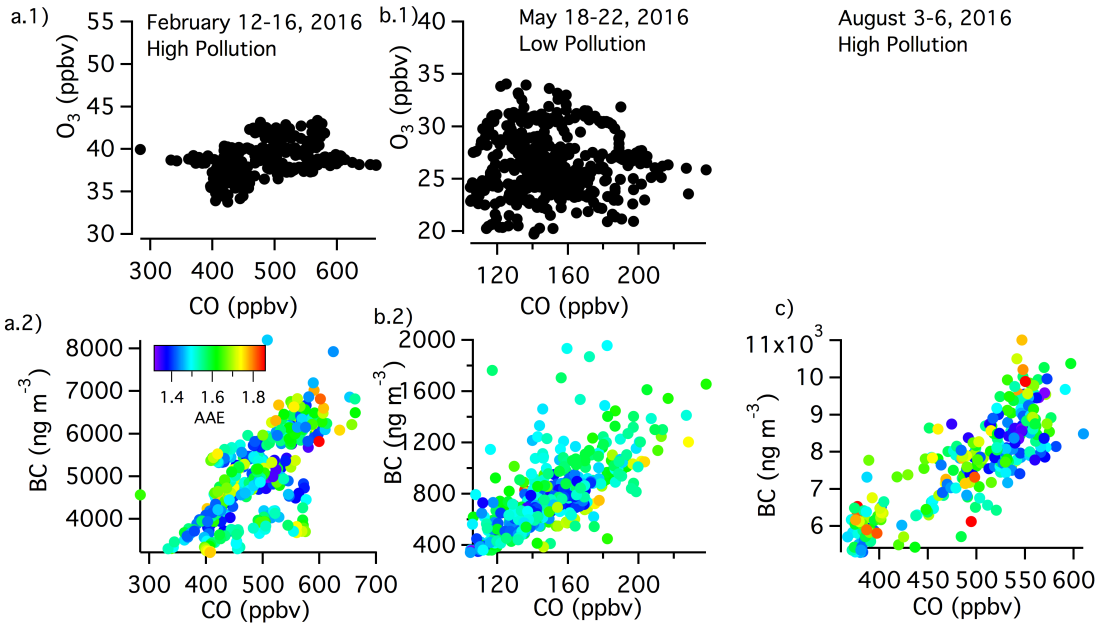

Figure 9: Polluted period in DJF (a), non-polluted period in MAM (b), and polluted period in JJA (c). Comparison of O3 and CO in a.1 and b.1, and comparison of BC and CO, color-coded by AAE, in a.2, b.2, and c for each respective period.

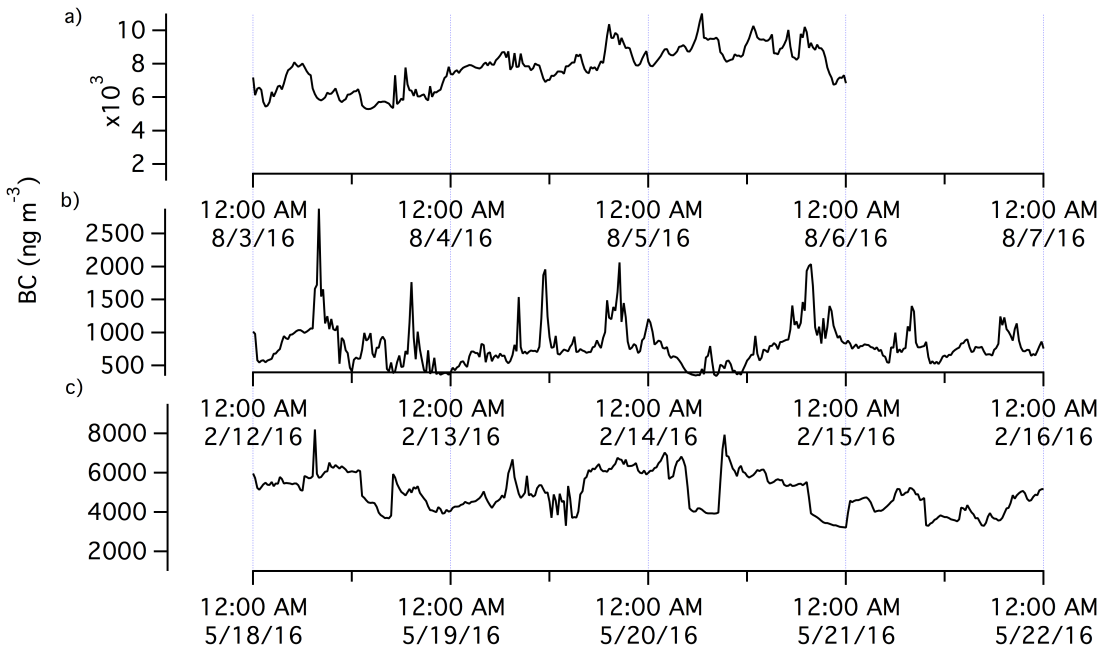

Figure 10: Case study of BC in a polluted period in August (a), a non-polluted period in May (b), and a polluted period in February (c).

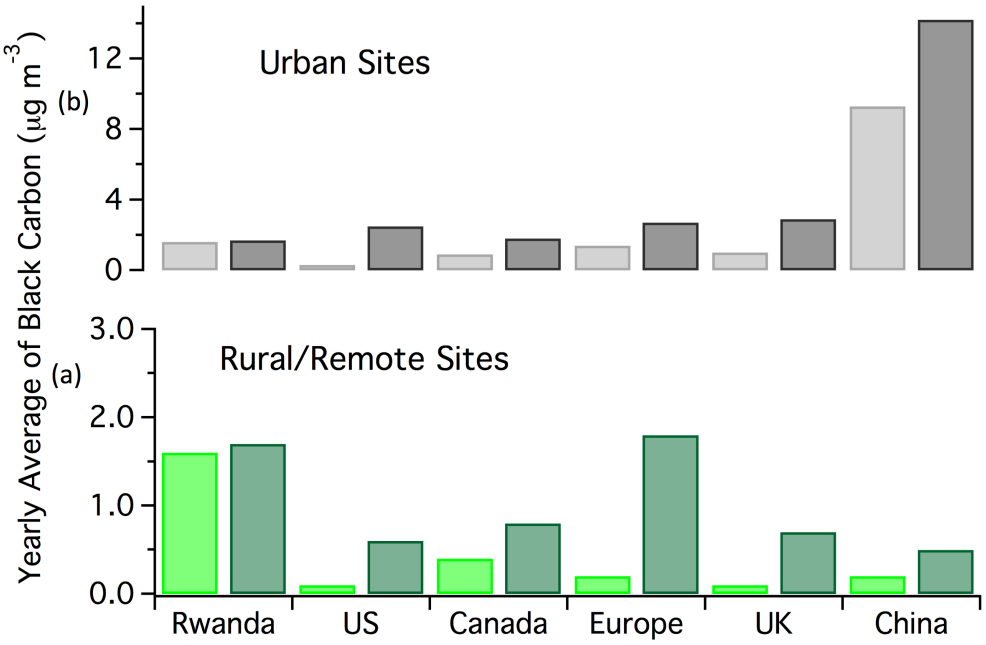

Figure 11. (a) Urban and (b) rural maximum (dark grey/green) of annual averages (dark grey/green) and minimum (light grey/green) of annual averages (light grey/green) BC concentrations at various sites globally. The BC data for Rwanda is from one location (Mt. Mugogo, rural), while the data for other locations were from multiple locations, averaged over one year. The annual average BC concentrations for Rwanda were calculated for the data from April 1st to April 1st of the next year. There was BC data for two years measured at RCO. BC data source for other sites: https://www3.epa.gov/blackcarbon/2012report/Chapter5.pdf, compiled from multiple sources.

925

926
927
928

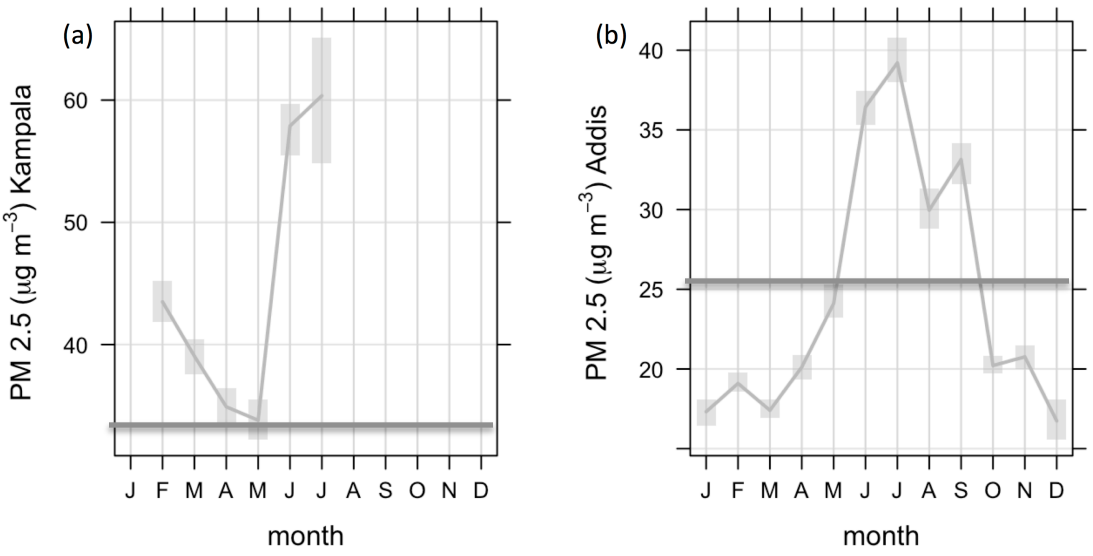

929
930 **Figure 12**: Monthly means of PM2.5 concentrations measured at the US Embassies in

931 (**a**) Kampala, Uganda (as available) and (**b**) Addis Ababa, Ethiopia (right) from

932 January-December 2016/2017 (as available). Shaded areas are 95% confidence

933 intervals. Lines indicate daily average WHO recommendation for healthy PM2.5 limits.

934